Taylor & Francis
Taylor & Francis Group

Experimental and simulated top electrode voltage in free-running oscillator radio frequency systems

H. Zhu[a], Z. Huang[a] and S. Wang[a,b]*

aCollege of Mechanical and Electronic Engineering, Northwest A&F University, Yangling, Shaanxi 712100, China; bDepartment of Biological Systems Engineering, Washington State University, Pullman, WA 99164-6120, USA

Top electrode voltage of a radio frequency (RF) heating system is an important parameter to accurately determine final sample temperatures using computer simulation. The purpose of this study was to establish the correlation between the top electrode voltage obtained by analytical method or simulation and the measured electrical currents. A measuring circuit was designed and developed to directly measure the top electrode voltage in the 27 MHz 6 kW RF unit together with the anode current read from the RF generator. The top electrode voltage was experimentally determined with 3 kg soybeans under five electrode gaps using computer simulation based on the matched temperature profiles in three layers, and analytical methods based on the heating rates measured by infrared camera, fiber optic sensors and thermocouples. Results showed that the electrode voltage decreased with increasing electrode gap or decreasing heating rate. The correlation between the electrode voltage estimated by temperature distributions from three-layer thermal imaging and the electrical currents both from the anode reading and direct measurement was the best one among the estimation methods and could be used for future computer simulations.

Keywords: RF; dielectric heating; top electrode voltage; soybean; finite element simulation; heating rate

1. Introduction

Free-running oscillator radio frequency (RF) heating systems are widely used in industrial applications and laboratory studies, such as post-baking,[1] drying,[2–4] disinfestations,[5–7] tissue heating [8,9] and pasteurization.[10,11] One of the biggest problems associated with RF heating is non-uniformity,[12] which may result in either unacceptable microbial survivals or food-quality degradations. To improve final temperature distributions in RF heated products, computer simulation models have been extensively applied to examine the causes of non-uniform heating and optimize the treatment protocol parameters.[13] In a simulation of RF heating, one of the most important parameters is the input voltage of top electrode, which clearly influences the electromagnetic field intensity in materials.[14] Overestimation or underestimation of top electrode voltage would result in misleading simulation results on the absorbed power density and final temperature in RF heated products.[15] Therefore, it is

---

*Corresponding author. Email: shaojinwang@nwsuaf.edu.cn

important to precisely determine the top electrode voltage in a given configuration of RF heating for effective computer simulation.

The top electrode voltage is generally influenced by the electrode design, electrode gap and load condition. This voltage has not been measured directly during RF heating but determined by indirect estimation methods. Marshall and Metaxas [15] estimated electrode voltages to be 7000–13,000 V for the RF-assisted heat pump drying of crushed brick. Birla et al. [12] developed one-dimensional analytical model to calculate the voltage using heating rate based on the uniform RF energy absorption without ambient heat loss and estimated the input voltage to be 8162 V when the 1% gel slab was heated in a RF system with an electrode gap of 160 mm. Using the same analytical method, Jiao et al. [16] reported 17,000 V for the top electrode during RF heating of 50 ml salt solution with an electrode gap of 110 mm. Tiwari et al. [13] and Alfaifi et al. [14] estimated the top electrode voltage using direct comparison of the final product temperature distributions between the experiment and simulation by inputting different voltage values. They found 4100 V for RF heating of 3 kg raisins at an electrode gap of 136 mm [14] and 13,000 V for 1 kg of RF-treated wheat flour at an electrode gap of 155 mm.[13] Although varying only by 7% between standby and full load during RF heating,[15] a general trend with the RF setting and load conditions may not be obtained by the reported data. It is desirable to develop a generally reliable and accurate method for estimating the top electrode voltage of RF heating systems used in computer simulation.

Objectives of this research were to: (1) measure the top electrode voltage using a custom-designed electrical circuit, (2) determine the top electrode voltage under five different electrode gaps using analytical method and finite element software based on the surface and internal temperature distributions in RF-heated soybeans with an infra-red camera, fiber optic sensors and thermocouples and (3) establish the correlation between the top electrode voltage obtained by analytical method or simulation and the anode current read from the RF unit or the measured current by the designed electrical circuit.

2. Materials and methods

2.1. Materials and RF heating systems

Soybeans were selected in this study due to available source, and known thermal and dielectric properties. The samples were purchased from a local grocery store, Yangling, China. The original moisture content of soybean was 4.7% on wet basis (w.b.) determined by a standard oven method.[17]

A 6 kW, 27.12 MHz parallel-plate RF heating system (SO6B, Strayfield International, Wokingham, UK) was used in this study. The top plate electrode size was 400 mm (W) × 830 mm (L), and the feed strip was located at the middle of the backside on the top electrode plate shown in Figure 1. The electrode gap was adjusted to obtain the different values of anode current and thus, the top electrode voltage. The measuring point of electrode voltage was selected at the geometric centre of the electrode plate (Figure 1). Anode current indicates the main output RF power from the generator or the top electrode voltage, which is dependent upon the properties of the load and electrode gaps.[15] An ammeter that measures the anode current (A) was provided by the RF manufacturer and installed on the back door of the RF generator.
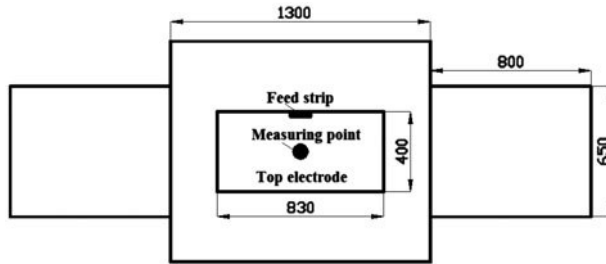
Figure 1. Top view of the RF system with the feeding and measuring points on the top electrode. All dimensions are in mm.

2.2. Calculation and simulation of top electrode voltage

2.2.1. Analytical method

The top electrode voltage (V, V) can be calculated by the analytical method [12]:

$$V = \left(d_{air}\sqrt{(\varepsilon')^2 + (\varepsilon'')^2} + d_{mat} \right)\left(\sqrt{\frac{\rho c_p}{\pi f \varepsilon_0 \varepsilon''}\frac{dT}{dt}} \right) \tag{1}$$

where, d_{air} and d_{mat} are air gap and material thickness (m); ε' and ε'' are dielectric constant and loss factor of soybeans; ρ and c_p are the density (kg m^{-3}) and specific heat (J kg^{-1} K^{-1}) of soybeans, respectively; dT/dt is the average heating rate (°Cs^{-1}) of soybeans over the heating volume.

The dielectric properties and thermal properties of soybeans were obtained from [18–20], respectively, and they are listed in Table 1. The top electrode voltage was calculated with Equation (1) by inputting the average heating rate estimated using different temperature measurement methods, such as fiber optic sensors, thermocouples and thermal imaging cameras. Since the RF heating profile was linearly proportional to the heating time, the heating rate was estimated by dividing the final sample temperature by the heating time at each electrode gap.

2.2.2. Computer simulation

A finite element software COMSOL (V4.3a, COMSOL Multiphysics, Burlington, MA, USA) was used to simulate the heating behaviour of RF systems using Joule heating model. The dielectric properties at 27.12 MHz and the thermal properties of the

Table 1. Thermal and dielectric properties of materials used in the computer simulation.

	Soybean	Polypropylene container[c]	Air[c]
Density (kg/m^3)	756	900	1.2
Heat capacity (J/kg K)	1722[b]	1800	1200
Thermal conductivity (W/m K)	0.1[b]	0.2	0.025
Dielectric constant	2.3[a]	2.0	1.0
Dielectric loss factor	0.13[a]	0.0023	0.0

[a]Guo et al. [18].
[b]Deshpande and Bal [20], Deshpande et al. [19].
[c]COMSOL material library.[23].

container (polypropylene), the sample (soybean) and the surrounding medium (air) are listed in Table 1 for simulation. The initial sample temperature was set at room temperature of 25 °C. Only the top surface of soybean samples was uncovered and exposed to air, and the sides and bottom were covered by a plastic rectangular container. The convective heat transfer coefficient of the top surface was set as $20 \, \text{W} \, \text{m}^{-2} \, °\text{C}^{-1}$ for natural convection.[14] The metal enclosure boundary of the RF unit was considered as thermal insulation ($\nabla T = 0$). The top electrode was set as the electromagnetic source since it introduced high frequency electromagnetic energy from the generator to the heating cavity and the bottom electrode was set as ground ($V = 0$ V). Detailed geometrical and electrical boundary conditions of RF systems used in the simulation could be found in Tiwari et al. [13] and Alfaifi et al. [14].

The simulation model was solved on a Dell workstation with two Dual Core 3.10 GHz Xeon processors, 8 GB RAM on a Windows 7 64-bit operating system. Fine tetrahedral mesh was generated in the soybean sample and the top electrode to guarantee the accuracy of temperature distribution results. Other parts of the system were meshed with normal size tetrahedral meshes. Mesh size was chosen based on the convergence study when the difference in the resulted temperatures between successive calculations was less than 0.1%. The initial and maximum time steps used in this study were set as 0.001 and 1 s. As reported by Tiwari et al. [13] and Alfaifi et al. [14], the top electrode voltage was estimated by computer simulation when the simulated temperature patterns and values matched well with the experimental temperature distributions in three layers of samples mapped with thermal imaging cameras under each electrode gap. After inputting various electrode voltages, the matching degree was finally evaluated by comparing the average temperature difference between simulation and experiment over three layers.

2.3. Measuring device and methods

A measuring device was designed in this study to directly measure the top electrode voltage. This circuit mainly consisted of voltage divider, filter and measuring parts (Figure 2). To reduce transmission impedance, the connection between the top electrode and measuring device was made by a rigid copper bar with 3 mm (H) × 50 mm (W) dimensions. A high-frequency ceramic capacitor of 50 pF was used together with 1 pF capacitor as an element of voltage divider of the measuring device. The major part of the measuring device (divider and filter circuits) was placed inside the RF oven and grounded well, but the measuring circuit (ammeter) was located outside the oven to prevent interference from the high electromagnetic field intensity. A well-shielding cable was used to connect the two parts of the measuring device. Since it is difficult to
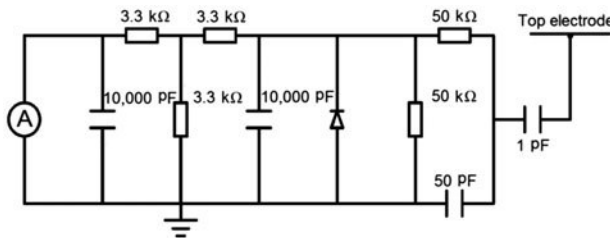

Figure 2.   The electric circuit for measuring the current from top electrode of the RF system.

accurately measure the impendence from the entire circuit, the electrical current (A) determined in the measuring circuit could be a reference value proportional to the top electrode voltage. This measured current could be used to establish the relationships with the voltage estimated by the analytical method and simulation model above, and further compare with the regressed equation from the anode current under five different electrode gaps.

2.4. *RF heating and temperature measurement*

RF heating was conducted in a polypropylene container (300 mm L × 220 mm W × 85 mm H) filled with 3 kg of soybeans (thickness of 60 mm with a bulk density of 756 kg m^{-3}) at a room temperature of 25 °C. The soybeans in the container were divided into three layers and separated by two thin gauzes (with mesh opening of 1 mm) to easily map the sample temperatures at heights of 2, 4 and 6 cm (Figure 3).

To cover the possible heating rates and achieve similar final average temperatures around 52 °C, five electrode gaps (110, 115, 120, 125 and 130 mm) were selected together with the corresponding RF heating times of 4.5, 5.5, 6.5, 7.5 and 8.5 min, respectively. These heating times were determined by online temperature detection using fiber optic sensors (FTS-P104, HeQi Opto-Electronic Technology, Xi'an, Shaanxi, China) with an accuracy of ±1 °C. Since the sample temperature distributions were non-uniform throughout the container and the fiber optic system had only six channels, four thermocouples (HH-25TC, Type-T, OMEGA Engineering Inc., Stamford, Connecticut, USA) with an accuracy of ±0.5 °C were used as additional temperature measurement points in the central part for obtaining a representative heating rate to estimate the top electrode voltage using analytical methods. During the RF heating, five sample temperatures at the height of 4 cm were measured by fiber optic sensors (Figure 3). The corresponding currents from both the measuring device and the anode ammeter were recorded. After RF heating was terminated at the predetermined time at each gap, the container was immediately moved out for surface temperature mapping in three layers using a thermal imaging camera (DM63, Dali Science and Technology, Hangzhou, Zhejiang, China) with an accuracy of ±2 °C and internal sample temperature measurements at four locations (Figure 3) using thermocouples. Each test was repeated two times.
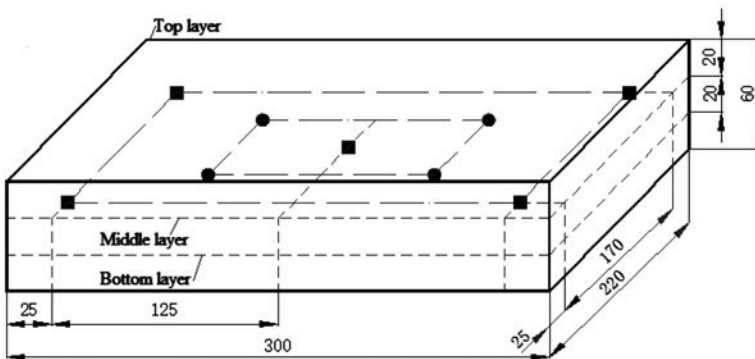

Figure 3. Temperature measurement locations of fiber optic sensors (■), thermocouples (●) and layers for infrared imaging camera in the sample container. All dimensions are in mm.

3. Results and discussion

3.1. *Anode current as influenced by electrode gaps*

Figure 4 shows the anode current as influenced by the electrode gap. Anode current decreased rapidly with increasing electrode gap. The maximum and minimum anode currents reached 0.38 and 0.31 A at electrode gaps of 110 and 130 mm, respectively. The trend was similar to that observed in Jiao et al. [21] and Wang et al. [4]. But the absolute value of anode currents was lower than that reported by Jiao et al. [21], and Marshall and Metaxas [15] which was probably caused by relatively lower moisture content of the samples in this study.

3.2. *Electrode voltage determined by simulation*

The electrode voltage was determined by computer simulation based on the similar temperature patterns and close final temperature values to those obtained in experiments at each electrode gap. Figure 5 shows an example of the contour plot of temperature distribution obtained by experiment and computer simulation at the gap of 120 mm. Both simulated and experimental results showed similar heating patterns in RF-treated soybeans at the top and middle layers. Although the heating pattern with general corner and edge heating in the bottom layer was observed both in computer simulation and experiment, the sample temperature in the experiment was clearly lower than that in the simulation where the larger areas of 55 and 60 °C in the corner and of 50 °C in the central part existed (Figure 5). This was probably caused by heat loss from the bottom due to close contact with the cooler bottom electrode plate and also from samples to the environment due to later measurements after the top and middle layers. The similar temperature distribution was also reported in RF-treated walnuts and legumes,[6,22] raisins [14] and wheat flour.[13] The average temperature difference values between simulation and experiment over three layers were 0.51, 0.35 and 0.79 °C for the given voltages of 5400, 5450 and 5500 V, respectively, at the electrode gap of 120 mm. Thus, 5450 V was determined for the gap of 120 mm and the simulated voltages at other gaps
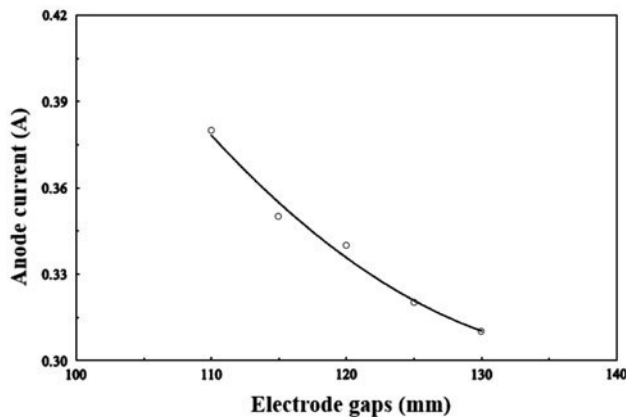
Figure 4. Anode current as a function of electrode gaps with a load of 3 kg soybeans at 4.7% (w.b.) moisture content.
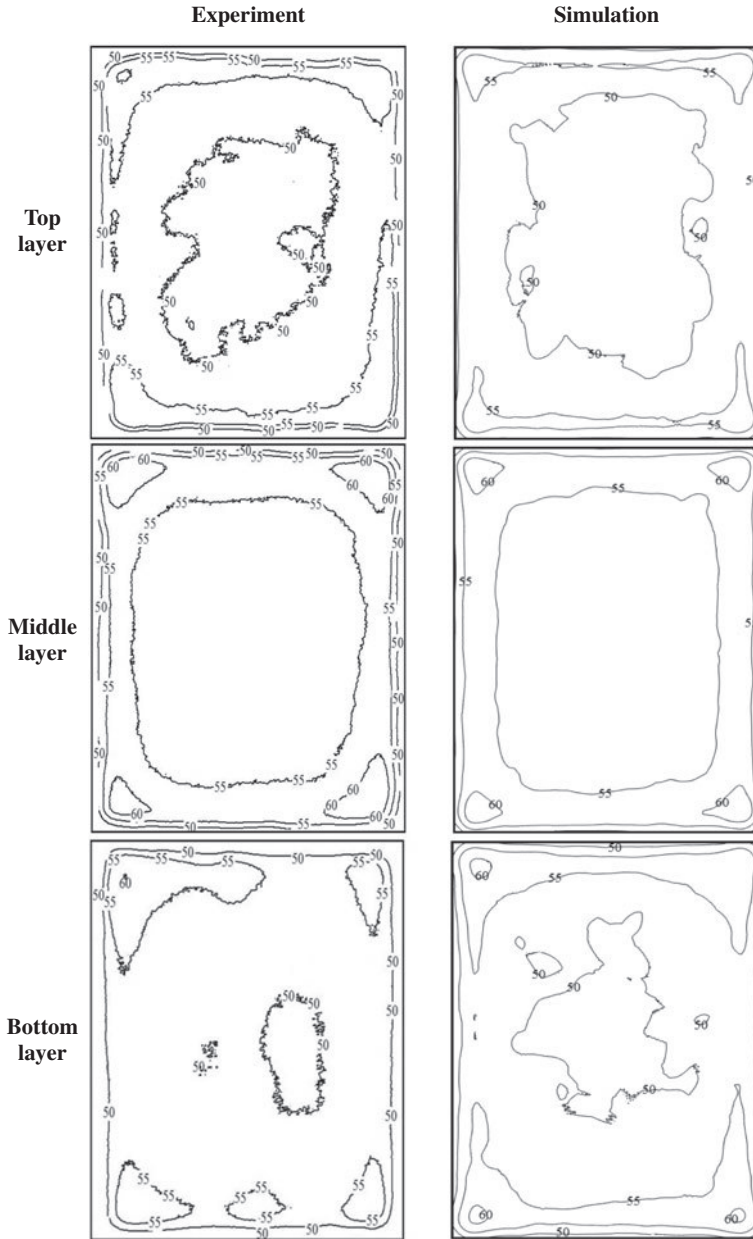
Experiment   Simulation

Top layer

Middle layer

Bottom layer

Figure 5.   Experimental and simulated temperature (°C) distributions in top, middle, and bottom layers (20, 40, and 60 mm from the bottom of sample) of soybeans placed in a polypropylene container after 6.5 min RF heating at an electrode gap of 120 mm.

obtained by the same method were plotted against the electrode gap (Figure 6). The results showed that the electrode voltage decreased linearly with increasing electrode gap, which was caused by the reduced RF power coupled into the sample.
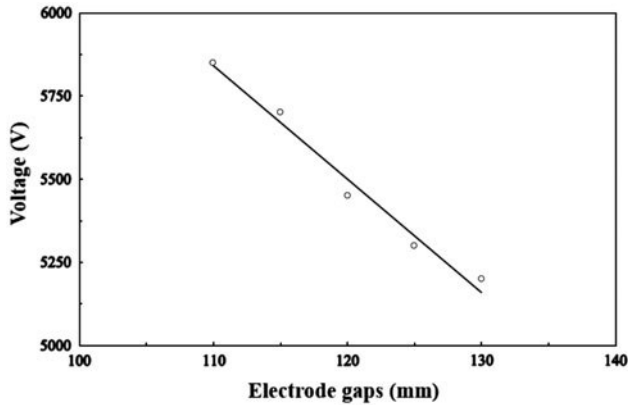
Figure 6. Simulated voltage as a function of electrode gaps with a load of 3 kg soybeans.

3.3. Electrode voltage determined by analytical method based on temperature measurements

Table 2 lists the final temperature and heating rate of soybeans obtained by different measurement methods and the resultant electrode voltage after RF heating at the given five electrode gaps. The results showed that the heating rate and the top electrode voltage decreased with increasing electrode gap for each measurement method. The final sample temperature was lowest using thermocouples in the centre of the second

Table 2. Final temperature, heating rate, and electrode voltage (average ± standard deviation over two replicates) obtained by different measurement methods after RF heating of 3 kg soybeans at the given 5 electrode gaps.

Gap (mm)	Measuring method	Final temperature (°C)	Heating rates (°C min^{-1})	Voltage (V)
110	Thermocouples	51.0 ± 0.6	5.8 ± 0.1	5991.4 ± 40.8
	Fiber optic	53.6 ± 4.7	6.6 ± 0.1	6411.2 ± 49.5
	Infrared-mid layer	55.2 ± 3.0	6.7 ± 0.4	6463.4 ± 207.4
	Infrared-3 layers	52.9 ± 3.3	6.2 ± 0.0	6216.7 ± 50.3
115	Thermocouples	51.3 ± 0.4	4.8 ± 0.1	5818.7 ± 48.8
	Fiber optic	55.7 ± 5.4	5.7 ± 0.2	6362.9 ± 94.3
	Infrared-mid layer	54.8 ± 3.3	5.4 ± 0.0	6190.9 ± 5.9
	Infrared-3 layers	53.3 ± 3.7	5.2 ± 0.1	6038.0 ± 45.6
120	Thermocouples	51.3 ± 0.3	4.0 ± 0.1	5669.8 ± 99.4
	Fiber optic	55.0 ± 5.1	4.7 ± 0.0	6102.4 ± 30.5
	Infrared-mid layer	54.0 ± 3.0	4.5 ± 0.1	5962.8 ± 81.5
	Infrared-3 layers	52.5 ± 3.3	4.2 ± 0.1	5803.0 ± 83.7
125	Thermocouples	49.6 ± 0.8	3.3 ± 0.0	5409.2 ± 5.8
	Fiber optic	53.6 ± 4.7	4.0 ± 0.0	5958.5 ± 19.1
	Infrared-mid layer	53.4 ± 3.3	3.8 ± 0.2	5814.8 ± 171.4
	Infrared-3 layers	52.1 ± 3.3	3.6 ± 0.2	5669.0 ± 169.1
130	Thermocouples	48.1 ± 0.1	2.7 ± 0.0	5193.8 ± 4.0
	Fiber optic	52.5 ± 4.9	3.4 ± 0.0	5807.5 ± 7.3
	Infrared-mid layer	51.6 ± 4.1	3.1 ± 0.1	5571.8 ± 106.0
	Infrared-3 layers	50.8 ± 4.5	3.0 ± 0.1	5476.4 ± 122.3

layer, which were located in the cold spots of the contour heating plot as shown in Figure 5, resulting in lowest heating rates and top electrode voltages. However, the sample temperatures measured by the fiber optic sensors and infrared camera in the mid layer were the highest since they were located in hot spots, such as corners and the mid layer (Figure 5). Generally, the resultant top electrode voltage could be representative for the average sample temperature measured by the infrared camera from three layers since this covered most of the heating patterns over the volume.

3.4. *Estimation of the top electrode voltage*

As expected, the top electrode voltage increased linearly with increasing anode current with high coefficient of determination (>0.91) (Figure 7(a) and Table 3) both for simulation and analytical methods. The general voltage difference varied between 432 and 613 V among the five estimation methods at different currents, resulting in less than 10% relative error. The voltage difference was mainly caused by the different measuring points and the simulation accuracy. The highest voltage resulted from fiber optic sensors, followed by infrared mid layer, infrared three layers and thermocouples, and the lowest one appeared from the computer simulation. Poor correlation was observed for the calculation based on the fiber optic sensors, which was probably caused by high
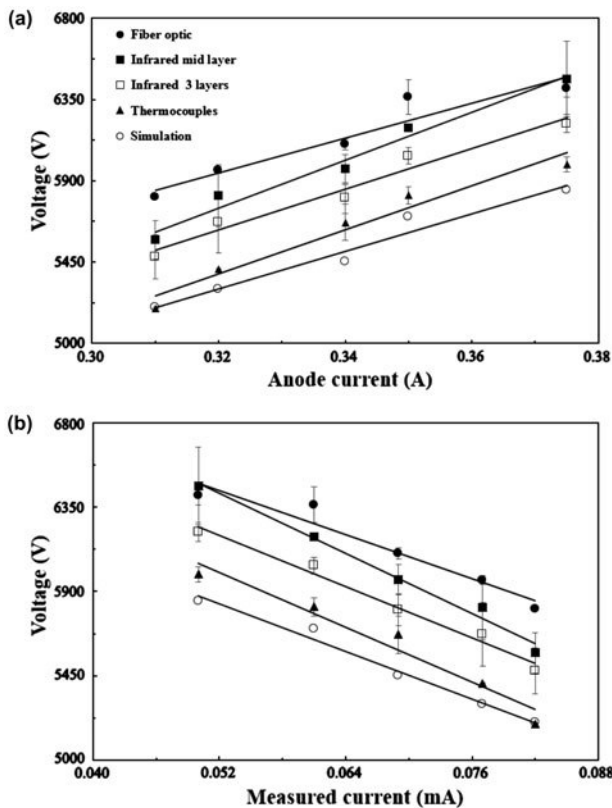

Figure 7. Correlations between the electrode voltages obtained by simulation or analytical methods based on the measured heating rate and the anode current (a) or measured current (b).

Table 3. Regression equations with coefficient of determination (R^2) between the top electrode voltage V (V) from computer simulation or analytical method based on the measured heating rates and the currents from the anode ammeter and the measuring device.

Method	Regression	From anode current I_a (A)	From directly measured current I_m (A)
Simulation	Equation	$V = 10401 \times I_a + 1974.1$	$V = -21128 \times I_m + 6932.5$
	R^2	0.9607	0.9848
Fiber optic	Equation	$V = 9644 \times I_a + 2858.9$	$V = -19637 \times I_m + 7459.9$
	R^2	0.9111	0.9382
Thermocouples	Equation	$V = 12203 \times I_a + 1479.8$	$V = -24422 \times I_m + 7272.4$
	R^2	0.9611	0.9562
Infrared 3 layers	Equation	$V = 11242 \times I_a + 2029.9$	$V = -22760 \times I_m + 7384.2$
	R^2	0.9653	0.9828
Infrared mid layer	Equation	$V = 13238 \times I_a + 1513.0$	$V = -26394 \times I_m + 7413.4$
	R^2	0.9763	0.9820

temperature variations from five locations (Table 3). This method also resulted in the overestimation of the electrode voltage since the four temperatures obtained were from the hottest corners in the relatively hot layer (mid layer). The sensor locations at four corners and one centre should be avoided to precisely estimate the top electrode voltage. The low top electrode voltage estimated from the thermocouples was probably caused by the low temperatures located in the central parts of the middle layer. The lowest top electrode voltage resulted from simulation seemed underestimated, especially for high anode current or RF power. This could be caused by the overestimation of the final sample temperatures in computer simulation which compromised the estimation of the simulated final temperature distributions from three layers as compared to the experimental ones, although the heating patterns in the top and middle layers were mainly considered as shown in Figure 5. Generally, the estimated top electrode voltage based on the heating rate measured by thermal imaging camera over three layers was located in the middle range among the used methods with $R^2 > 0.97$, which could really represent the average heating rate over the whole volume of the samples and reduce the relative error to less than 5% from other estimation methods. This resulted correlation between the voltage and the anode current could be used for future computer simulation.

The directly measured current was negatively proportional to the top electrode voltage (Figure 7(b)), which was inversely different from the correlation between the top electrode voltage and the anode current (Figure 7(a)). The correlation based on the directly measured current was better than that based on the anode current due to slightly higher R^2 (Table 3). The effect of different methods on the correlation based on the measured current was similar to that based on the anode current as described above. As soon as the electrical currents were obtained either by the anode reading or the measuring device in a given RF heating, the top electrode voltage could be precisely estimated by the relation established in this study based on the temperature measurements using thermal imaging camera from three layers. This estimation method based on the measured currents could provide rapid and accurate top electrode voltage as compared to simulation and analytical methods through sophisticated temperature mapping.

The correlations ($V = 11242 \times I_a + 2029.9$ and $V = -22760 \times I_m + 7384.2$) from three-layer temperatures were finally suggested to estimate the electrode voltage when

inputting the anode and measured currents, which could be easily and quickly obtained from the current meters. The voltage precision depended on the reading accuracy of the current value, which needed to ensure three decimal point readings from the current meters. The estimated electrode voltage in this study ranged between 5514 and 6246 V when the anode and measured current were from 0.310 to 0.375 A, and from 0.050 to 0.082 mA, respectively. The measured current could be only used to measure the maximum voltage (7384 V) but the anode current was able to measure the maximum voltage up to 13,272 V when $I_a = 1.0$ A, which covered 13,000 V for the RF drying of crushed brick reported by Marshall and Metaxas [15] and RF treated 1 kg wheat flour reported by Tiwari et al. [13]. The further validation studies could be conducted with larger electrode gaps to obtain lower voltage and with smaller gaps and bigger loads (e.g. higher moisture contents or heavier samplers) to reach higher voltages.

4.　Conclusions

Top electrode voltage was studied using both computer simulation and experimental methods. A custom-made measuring device was developed to measure the electrical current, which was thus used to estimate the voltage of the top electrode. The results showed that the heating rate and the top electrode voltage decreased with increasing electrode gap for analytical methods. The resultant top electrode voltage could be acceptable by analytical methods based on the heating rate measured by the infrared camera from three layers since this could really represent the average temperature over the whole volume of the samples. The top electrode voltage was linearly proportional to the anode current and the directly measured current with high coefficient of determination ($R^2 > 0.91$) both for simulation and analytical methods. The correlation based on the directly measured current was better than that based on the anode current due to slightly higher R^2. The anode current or the directly measured current could be applied to precisely and quickly estimate the top electrode voltage used for computer simulation.

References

[1] Koral T. Radio frequency heating and post-baking. Biscuit World Iss. 2004;7. Available from: http://www.strayfield.co.uk/images/radio_frequency.pdf
[2] Marshall M, Metaxas A. Radio frequency assisted heat pump drying of crushed brick. Appl. Therm. Eng. 1999;19:375–388.
[3] Lee NH, Li C, Zhao XF, Park MJ. Effect of pretreatment with high temperature and low humidity on drying time and prevention of checking during radio-frequency/vacuum drying of Japanese cedar pillar. J. Wood Sci. 2010;56:19–24.

[4] Wang Y, Zhang L, Johnson J, Gao M, Tang J, Powers J, Wang S. Developing hot air-assisted radio frequency drying for in-shell macadamia nuts. Food Bioprocess Technol. 2013;1:1–11.

[5] Lagunas-Solar M, Pan Z, Zeng N, Truong T, Khir R, Amaratunga K. Application of radiofrequency power for non-chemical disinfestation of rough rice with full retention of quality attributes. Appl. Eng. Agric. 2007;23:647–654.

[6] Wang S, Monzon M, Johnson J, Mitcham E, Tang J. Industrial-scale radio frequency treatments for insect control in walnuts: I: heating uniformity and energy efficiency. Postharvest Biol. Technol. 2007;45:240–246.

[7] Wang S, Monzon M, Johnson J, Mitcham E, Tang J. Industrial-scale radio frequency treatments for insect control in walnuts: II: insect mortality and product quality. Postharvest Biol. Technol. 2007;45:247–253.

[8] Rajhi A. Optimization of the EM heating cycle by using a dual frequency local hyperthermia applicator. J. Electromagn. Waves Appl. 2003;17:447–464.

[9] Mohsin SA, Sheikh NM, Abbas W. MRI induced heating of artificial bone implants. J. Electromagn. Waves Appl. 2009;23:799–808.

[10] Gao M, Tang J, Villa-Rojas R, Wang Y, Wang S. Pasteurization process development for controlling *Salmonella* in in-shell almonds using radio frequency energy. J. Food Eng. 2011;104:299–306.

[11] Kim S-Y, Sagong H-G, Choi SH, Ryu S, Kang D-H. Radio-frequency heating to inactivate *Salmonella typhimurium* and *Escherichia coli* O157:H7 on black and red pepper spice. Int. J. Food Microbiol. 2012;153:171–175.

[12] Birla S, Wang S, Tang J. Computer simulation of radio frequency heating of model fruit immersed in water. J. Food Eng. 2008;84:270–280.

[13] Tiwari G, Wang S, Tang J, Birla S. Computer simulation model development and validation for radio frequency (RF) heating of dry food materials. J. Food Eng. 2011;105:48–55.

[14] Alfaifi B, Tang J, Jiao Y, Wang S, Rasco B, Jiao S, Sablani S. Radio frequency disinfestation treatments for dried fruit: model development and validation. J. Food Eng. 2014;120:268–276.

[15] Marshall M, Metaxas A. Modeling of the radio frequency electric field strength developed during the RF assisted heat pump drying of particulates. J. Microwave Power Electromagn. Energy. 1998;33:167–177.

[16] Jiao Y, Tang J, Wang S, Koral T. Influence of dielectric properties on the heating rate in free-running oscillator radio frequency systems. J. Food Eng. 2014;120:197–203.

[17] SAC. Inspection of grain and oilseeds methods for determination of moisture content GB5497-85. Beijing: Standardization Administration of the People's Republic of China; 1985.

[18] Guo W, Wang S, Tiwari G, Johnson JA, Tang J. Temperature and moisture dependent dielectric properties of legume flour associated with dielectric heating. LWT-Food Sci. Technol. 2010;43:193–201.

[19] Deshpande S, Bal S, Ojha T. Bulk thermal conductivity and diffusivity of soybean. J. Food Process. Preserv. 1996;20:177–189.

[20] Deshpande S, Bal S. Specific heat of soybean. J. Food Process Eng. 1999;22:469–477.

[21] Jiao S, Johnson J, Tang J, Wang S. Industrial-scale radio frequency treatments for insect control in lentils. J. Stored Prod. Res. 2012;48:143–148.

[22] Wang S, Tiwari G, Jiao S, Johnson JA, Tang J. Developing postharvest disinfestation treatments for legumes using radio frequency energy. Biosyst. Eng. 2010;105:341–349.

[23] COMSOL. Material library V4.3a. Burlington (VT): COMSOL Multiphysics; 2012.